ORIGINAL ARTICLE

Topography of ¹¹C-Pittsburgh compound B uptake in Alzheimer's disease: a voxel-based investigation of cortical and white matter regions

Daniele de P. Faria,[1,2] (iD) Fabio L. Duran,[2,3] Paula Squarzoni,[2,3] Artur M. Coutinho,[1,2] Alexandre T. Garcez,[1,2] Pedro P. Santos,[2,3] Sonia M. Brucki,[4] Maira O. de Oliveira,[4] Eduardo S. Trés,[4] Orestes V. Forlenza,[2,5] Ricardo Nitrini,[4] Carlos A. Buchpiguel,[1,2] Geraldo Busatto Filho[2,3] (iD)

[1]Laboratório de Medicina Nuclear (LIM 43), Departamento de Radiologia e Oncologia, Faculdade de Medicina, Universidade de São Paulo (USP), São Paulo, SP, Brazil. [2]Núcleo de Apoio à Pesquisa em Neurociência Aplicada (NAPNA), USP, São Paulo, SP, Brazil. [3]Laboratório de Neuroimagem em Psiquiatria (LIM 21), Departamento de Psiquiatria, Faculdade de Medicina, USP, São Paulo, SP, Brazil. [4]Departamento de Neurologia, Faculdade de Medicina, USP, São Paulo, SP, Brazil. [5]Laboratório de Neurociências (LIM 27), Departamento de Psiquiatria, Faculdade de Medicina, USP, São Paulo, SP, Brazil. (iD) DPF https://orcid.org/0000-0002-1766-2786, (iD) GBF https://orcid.org/0000-0003-4749-4602

Objective: To compare results of positron emission tomography (PET) with carbon-11-labeled Pittsburgh compound B (¹¹C-PIB) obtained with cerebellar or global brain uptake for voxel intensity normalization, describe the cortical sites with highest tracer uptake in subjects with mild Alzheimer's disease (AD), and explore possible group differences in ¹¹C-PIB binding to white matter.

Methods: ¹¹C-PIB PET scans were acquired from subjects with AD (n=17) and healthy elderly controls (n=19). Voxel-based analysis was performed with statistical parametric mapping (SPM).

Results: Cerebellar normalization showed higher ¹¹C-PIB uptake in the AD group relative to controls throughout the cerebral cortex, involving the lateral temporal, orbitofrontal, and superior parietal cortices. With global uptake normalization, greatest cortical binding was detected in the orbitofrontal cortex; decreased ¹¹C-PIB uptake in white matter was found in the posterior hippocampal region, corpus callosum, pons, and internal capsule.

Conclusion: The present case-control voxelwise ¹¹C-PIB PET comparison highlighted the regional distribution of amyloid deposition in the cerebral cortex of mildly demented AD patients. Tracer uptake was highest in the orbitofrontal cortex. Decreased ¹¹C-PIB uptake in white-matter regions in this patient population may be a marker of white-matter damage in AD.

Keywords: Amyloid PET imaging; Alzheimer's disease; statistical parametric mapping

Introduction

Molecular brain imaging methods are clinically established tools to assist in the diagnosis of Alzheimer's disease (AD) and other neurodegenerative diseases, as well as help predict the risk of conversion from mild cognitive impairment (MCI) to AD dementia.[1,2] The most typical positron emission tomography (PET) findings supporting the diagnosis of AD include decreased regional brain glucose metabolism, affecting mainly the temporoparietal and posterior cingulate cortices, as assessed by fluorodeoxyglucose-PET (¹⁸F-FDG-PET),[3] and increased overall cortical uptake of radiotracers that bind to β-amyloid (Aβ) plaques, a molecular hallmark of AD, such as Pittsburgh compound B labeled with carbon-11 (¹¹C-PIB).[3,4]

Different methods for quantification of PET data have been employed in case-control studies assessing patterns of significantly increased brain uptake of amyloid imaging tracers in patients with AD. Most often, regions of interest (ROIs) placed on selected cortical portions or voxel-based methods that inspect the entire brain, such as statistical parametric mapping (SPM), have been used. By allowing unbiased, voxelwise investigations of the whole cerebral cortex, the SPM-based approach has the advantage of identifying the specific peak cortical sites where, on average, there is a greater degree of abnormal amyloid deposition in the brain of patients with AD compared to controls, as well as mapping the topography of brain regions spared by this pathological process.

A standard step in group-based brain PET studies consists in normalizing the intensity of a voxel (or the mean tracer uptake within an ROI) to a reference brain measure unaffected by the disease under investigation, thus accounting for inter-individual tracer uptake variations

caused by factors such as the dose of radiolabeled tracer injected intravenously (which is similar, but not exactly equal, across individuals). After intensity normalization, imaging data based on the concentration of radioactivity in a voxel or ROI inside the brain can be safely compared between groups. Case-control ^{18}F-FDG-PET studies of AD, for instance, have employed as reference measures either the mean tracer uptake in the whole brain or its uptake in a specific region unaffected by the neuropathological process, such as the cerebellum, pons, or sensorimotor cortex.[5-7]

Previous SPM-based analyses of ^{18}F-FDG-PET data showed high discrimination of patients with AD from healthy controls when using either global normalization (a procedure known as proportional scaling)[5] or the reference-region approach.[6,7] While the reference-region approach is usually more sensitive to uncover AD-related brain hypofunctional patterns compared to healthy controls in ^{18}F-FDG-PET studies,[6,7] whole-brain normalization may afford greater group discrimination specifically in AD-typical regions[7] and better differentiation between AD and other forms of dementia. The latter finding may be explained by the fact that the global normalization procedure highlights localized foci where decreased glucose uptake is present above the overall mean level of brain hypofunction, thus demonstrating the brain areas most impacted in each different dementia subtype.[6]

Since extensive cortical amyloid deposition is expected in AD cases, the reference-region approach is the method most often chosen for PET studies of AD using amyloid imaging tracers for voxelwise group comparisons.[5,8] Since post-mortem studies show low Congo-red and thioflavin-S staining in the cerebellum (suggesting a lack of amyloidosis), normalization of the cortical ^{11}C-PIB binding to cerebellar tracer uptake has become a standard procedure.[9,10] Nevertheless, one potential benefit of using proportional scaling for normalization of amyloid PET imaging data is the possibility to point out which brain regions have the highest abnormal level of cortical amyloid deposition (as in the ^{18}F-FDG studies reviewed above). This could help identify the brain areas most impacted by amyloid deposition in different dementia subtypes and correlate such findings with those seen in other PET imaging methods.[11] However, amyloid PET imaging studies of AD systematically comparing results obtained with the two different approaches for tracer uptake normalization have been scarce to date.

One other issue rarely explored in PET studies using amyloid imaging tracers regards the concurrent assessment of between-group differences in white- and gray-matter tracer uptake. The presence of pathological white-matter changes early in the course of AD is being progressively recognized,[12] and it has been demonstrated that ^{11}C-PIB has a high affinity for white matter.[4,13] Therefore, the use of PET with ^{11}C-PIB may potentially uncover white-matter foci of differential tracer uptake between patients with AD and healthy controls or subjects with other types of dementia.

In the present study, we used SPM to conduct a comparative analysis of ^{11}C-PIB-PET data obtained from a group of elderly patients with AD against age- and gender-matched healthy controls. Our aims were: to describe the topographical distribution of the cortical sites with highest tracer uptake in subjects with very mild or mild Alzheimer's dementia, based on the Clinical Dementia Rating (CDR)[14]; to compare results obtained with two different normalization approaches, respectively cerebellar grey matter uptake (as reference region) and global tracer uptake (proportional scaling); and to explore possible differences in ^{11}C-PIB binding to white matter between subjects with AD and healthy individuals.

Methods

Study population

Seventeen patients with AD and 19 healthy elderly volunteers were enrolled in the study. Approval was obtained from the ethics committee of Hospital das Clínicas, Faculdade de Medicina, Universidade de São Paulo (USP), Brazil (CAPPesq 368.037), and informed consent was obtained from all participants (or, in the AD group, their caregivers).

Patients with AD were recruited from outpatient memory clinics of the departments of Neurology (n=12) and Psychiatry (n=5) of Faculdade de Medicina, USP. All patients fulfilled the National Institute on Aging and Alzheimer's Association (NIA-AA) criteria for probable AD dementia.[15] All patients and at least one close family member underwent structured interviewing using the Structured Clinical Interview for DSM-IV (SCID-IV), translated and adapted to Portuguese,[16] to confirm the presence of dementia and investigate present or lifetime history of psychiatric disorders. The presence of consistent cognitive deficits compatible with the diagnosis of AD was documented by an extensive neuropsychological assessment, including tests evaluating episodic and semantic memory, attention, processing speed, language, and executive functioning. The clinical severity of dementia was assessed using the CDR scale,[14] the Blessed scale,[17] and the Mini-Mental State Examination (MMSE).[18] Finally, although we did not collect comprehensive biomarker data (Aβ deposition, pathologic tau, and neurodegeneration) to biologically characterize the AD continuum in accordance with the recent NIA-AA research framework, we classified our AD subjects using the numeric clinical staging scheme proposed in the framework.[19]

Healthy controls were recruited from activity centers and groups for elderly individuals in the community. They also underwent structured interviewing using the SCID-IV[16] and the extensive neuropsychological assessment described above; all controls displayed normal performance for their age range.

Subjects in the AD group had no history of neurologic or psychiatric disorders prior to the onset of dementia. Those with recent, non-stabilized depressive or anxiety disorders were also excluded. Subjects with past or current history of major psychiatric disorders and neurological conditions were also excluded from the control sample. Additional exclusion criteria for both the AD and healthy control groups were: presence of severe medical conditions or any systemic disorders associated

with cognitive impairment; family history of dementia with a dominant pattern of inheritance; auditory deficits or uncorrected visual impairments that could interfere with the cognitive evaluation; and brain lesions detected incidentally on magnetic resonance imaging (MRI). In both groups, family history of AD, as well as information about current and previous medical, neurological, and psychiatric illness, was obtained during the interview with the participants as well as from at least one close family member in the case of AD subjects.

Demographic data, clinical details, and main neuropsychological characteristics for the two groups were managed using the Research Electronic Data Capture (REDCap) method[20] and are provided in Table 1.

[11]C-PIB PET radiochemistry and image acquisition

Carbon-11 dioxide ([11]CO$_2$) was prepared by proton bombardment of nitrogen gas (N$_2$) with a trace amount of oxygen gas (O$_2$) 2% via the ^{14}N(p,α)^{11}C nuclear reaction using the PETtrace 880 cyclotron (GE Healthcare, Uppsala, Sweden). [11]CO$_2$ produced in the cyclotron was sent to a synthesis module (Modular-Lab, Eckert & Ziegler, Berlin, Germany), where it was hydrogenated to form methane ([11]CH$_4$). Methane was reacted with bromine to produce methyl bromide ([11]CH$_3$Br), which, in contact with a silver triflate column, formed methyl triflate ([^{11}C]MeOTf), which was used as the methylation agent.

[^{11}C]MeOTf was transferred to a reaction vial containing 1 mg of 2-(4′-aminophenyl)-6-hydroxybenzothiazole (ABX, Radeberg, Germany) and 0.7 mL of 2-butanone (Sigma-Aldrich, Darmstadt, Germany). The reaction mixture was heated at 80 °C for 90 seconds. After purification by high-performance liquid chromatography (HPLC), the product was formulated in ethanol 10% in saline and quality control performed. The product was released for human injection after quality control approval (radiochemical purity > 95%; specific activity > 20 GBq/μmol).

For image acquisition, patients were placed in a PET/ computerized tomography (CT) scanner (Discovery 710, GE Healthcare, Milwaukee, WI, USA). Before PET, a scout CT image was acquired at 120 kVp and 70 mA (140 mA and 0.5 s per rotation), reconstructed with the GE "PETAC" (highly smoothed) and GE "standard" (medium) filters, and used for attenuation correction. After CT, the patient's brain was positioned in the center of the field of view (FOV) of the PET scanner. ^{11}C-PIB, 296-740 MBq (8-20 mCi), was injected intravenously and PET imaging was begun immediately after the start of injection. ^{11}C-PIB PET images were acquired dynamically for 70 minutes. The images were corrected for attenuation, scatter, dead time, and decay, and reconstructed using the OSEM algorithm (VPHD, GE Healthcare, Milwaukee, WI, USA), using four iterations, 16 subsets, a cutoff filter of 3 mm, and point spread function modeling (SHARP IR, GE Healthcare, Milwaukee, WI, USA). For the present study, only images obtained from 40 to 70 minutes were used for analysis.[21] This was condensed in time to create a 30-minute static image. Illustrative time-activity curves (TACs) were made using PMOD™ version 3.4 (PMOD Technologies Ltd., Zurich, Switzerland).

No adverse effects or signs of allergic reactions were noted by the researchers conducting the image acquisition or reported by the participants or caregivers after the scans.

Structural magnetic resonance imaging (MRI) data acquisition

Anatomical MRI datasets were acquired using a Philips Achieva 3T scanner at Instituto de Radiologia, Hospital das Clínicas, Faculdade de Medicina da USP. A 3D T1-weighted scan was acquired using the following parameters: repetition time (TR) 7 ms, echo time (TE) 3.2 ms, flip angle 8°, Sense 1.5, FOV 240 × 240, matrix 240 × 240, 180 slices of 1 mm each with no gap, yielding a voxel size of 1 × 1 × 1 mm.

Table 1 Demographic and clinical characteristics of subjects with Alzheimer's disease and healthy controls

	Alzheimer's disease	Healthy controls	Statistical test	Significance
Sex, male:female	7:10	5:14	$\chi^2 = 0.348$	p = 0.5551
Age, years	74.9 (7.9)	73.5 (5.8)	t = 0.64	p = 0.5252
Range	61-87	65-84		
Handedness, right:left	16:1	19:0	$\chi^2 = 0.003$	p = 0.955
Years of education	8.5 (5.7)	14.0 (4.4)	t = 3.24	p = 0.0027
MMSE scores*	21.8 (4.8)	28.6 (1.3)	t = 5.703	p < 0.0001
Range	12-29	26-30		
CDR scores	0.9 (0.2)			
Range	0.5-1			
Blessed scores	5.9 (4.1)			
Range	0.5-14			

Data presented as mean (standard deviation), unless otherwise specified.
CDR = Clinical Dementia Rating; MMSE = Mini-Mental State Examination.
* Data missing for two patients with Alzheimer's disease.

Protocol for statistical parametric mapping (SPM) processing of ^{11}C-PIB PET images and PIB positivity criteria

Initially, ^{11}C-PIB-PET and T1-MRI datasets were converted from DICOM format to NIfTI format using DCM2NII software (http://www.cabiatl.com/mricro/mricron/dcm2nii.html). ^{11}C-PIB-PET images were co-registered to the T1-MRI datasets of the same individual using PMOD™ version 3.4. All images were oriented manually to place the anterior commissure at the origin of the three-dimensional Montreal Neurological Institute (MNI) coordinate system. Regarding ^{11}C-PIB-PET data, all images were corrected for partial volume effects (PVEs) to avoid confounding effects secondary to the degree of regional brain atrophy[22] and high white-matter uptake.[23] Thus, the co-registered ^{11}C-PIB-PET images were corrected for PVE through the Meltzer method,[24] an optimized voxel-based algorithm that is fully implemented in PVElab software (http://pveout.ibb.cnr.it/PVEOut_Software.htm).[25] Using SPM version 8 (Wellcome Trust Centre of Neuroimaging, London, United Kingdom) running in MATLAB R2012a (MathWorks, Natick, MA, USA), the T1-MRI datasets of each individual were then spatially normalized to the standard MNI space using diffeomorphic anatomical registration through exponentiated Lie algebra.[26] Subsequently, the steps used in the spatial normalization of T1-MRI datasets of each individual were applied to the PVE-corrected ^{11}C-PIB-PET images in order to achieve spatial normalization to MNI space.[27] Finally, the spatially normalized, PVE-corrected ^{11}C-PIB-PET images were smoothed using an 8-mm full-width-at-half-maximum (FWHM) Gaussian filter.

All subjects in the two groups were also classified individually as PIB-positive or negative using visual analysis by two experienced nuclear medicine physicians[28] assisted by automated methods (CortexID Suite® software, GE Healthcare), with a standardized uptake value ratio (SUVr) > 1.42 as the positivity criterion.[29]

Statistical analysis

For intensity normalization of PVE-corrected ^{11}C-PIB-PET images using tracer uptake in the cerebellum, we divided the value of each voxel by the average of the voxels belonging to a cerebellar ROI available in the Anatomical Automatic Labeling SPM toolbox (http://www.gin.cnrs.fr/AAL). Voxelwise comparisons of PIB uptake between groups were then conducted using *t* tests. The resulting statistics were initially considered with a threshold of $p < 0.001$; the cluster was reported as significant when surpassing the $p \leqslant 0.05$ level, family-wise error (FWE)-corrected for multiple comparisons over the whole brain and with a minimum cluster size of 10 voxels.

For between-group comparisons of PVE-corrected ^{11}C-PIB-PET data using intensity normalization to total tracer uptake in the brain, we used the proportional scale function available within SPM8. The same statistical inference approach described was employed.

Results

Clinical and social demographic data

The AD group (n=17, 10 females) had a mean age of 74.9±7.9 years and a mean educational level of 8.5±5.7 years of schooling. All but one of the 17 AD patients were right-handed. Ratings on the CDR scale were 0.5 in four cases and 1.0 in 13 cases. Patients in the AD group were classified as stage 4 (mild dementia) according to the current NIA-AA research framework.[19] Additional clinical and cognitive performance indices for the two groups are provided in Table 1. MMSE score data were missing for two AD patients; the mean score for the remaining individuals was 21.8±4.8. At the time of neuroimaging, 10 (58.8%) AD patients were on acetylcholinesterase inhibitors and seven (41.2%) were on antidepressants.

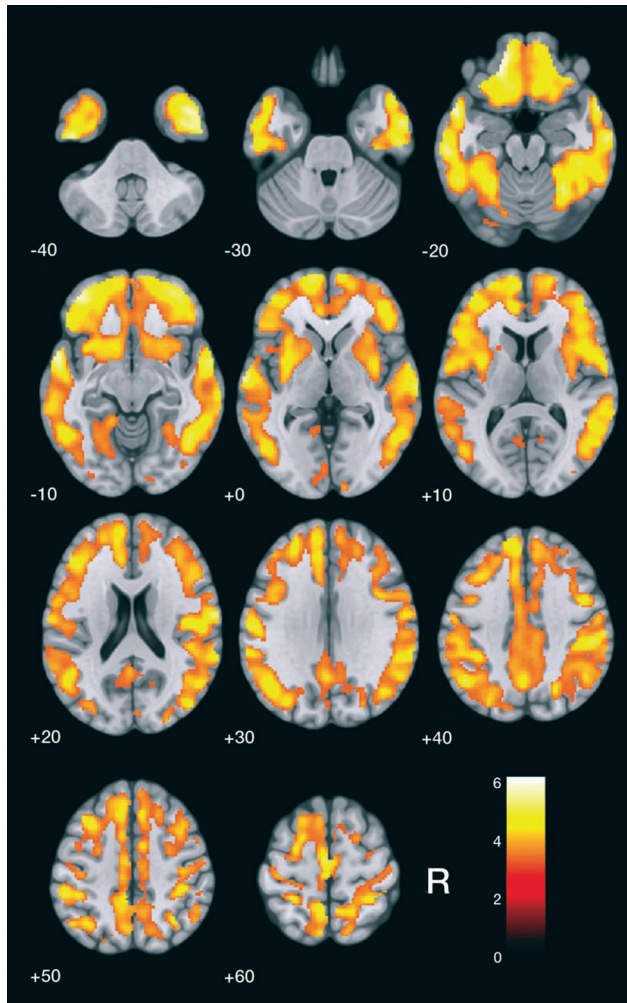The healthy control group (14 females) had a mean age of 73.5±5.8 years and an average 14.0±4.4 years of formal education. They had no memory complaints, and their physical and neurological examination was normal. The mean MMSE score was 28.6±1.3. All controls were right-handed.

The two groups were matched for age and gender, but AD patients displayed a significantly lower educational attainment compared to controls ($p = 0.0027$, Table 1).

Between-group comparisons of ^{11}C-PIB data: increased uptake in AD subjects relative to controls

When AD patients were compared to healthy controls using data normalized to uptake in the cerebellar gray matter, increased ^{11}C-PIB uptake (at the initial $p < 0.001$ threshold) was detected throughout the cerebral cortex, involving mainly the lateral temporal cortex, basal portions of the frontal cortex, and superior portions of the parietal cortex. Superior portions of the prefrontal cortex and the occipital cortex were less affected, and subcortical gray-matter structures were spared. This topographical profile is shown in Figure 1. Clusters of significant difference between groups (filtered at $p_{FWE} < 0.05$, corrected for multiple comparisons) are displayed in Table 2. Highest statistical significance was attained for a cluster located in the right superior parietal lobule; additional large clusters (> 200 voxels) with peak voxels located respectively in the left orbitofrontal cortex, left superior temporal gyrus, and right inferior temporal gyrus retained statistical significance, as well as nine other less-extensive clusters (< 100 voxels) in temporal, parietal, and basal frontal locations (Table 2).

Comparison of ^{11}C-PIB-PET data normalized to the total brain uptake between the two groups (at the initial $p < 0.001$ threshold) again showed several, though less extensive, cortical foci of increased tracer uptake in AD patients relative to controls, highlighting most prominently basal portions of the frontal cortex (Figure 2). Voxels of peak statistical difference between groups ($p_{FWE} < 0.05$, corrected for multiple comparisons) are displayed in Table 3, and show statistical significance of the same magnitude as seen in the analyses with data normalized to

increase of cortical uptake in patients with AD when compared to controls.

Between-group comparisons of ^{11}C-PIB data: decreased uptake in patients with AD relative to controls

With ^{11}C-PIB PET data normalized to cerebellar grey-matter uptake, a number of white-matter regions displayed reduced tracer uptake in patients with AD relative to controls at the uncorrected $p < 0.001$ statistical level of significance (all clusters with an associated z score greater than 3.30). However, none of those clusters retained statistical significance after FWE correction for multiple comparisons.

With ^{11}C-PIB PET data normalized to global brain uptake, the search for brain regions showing relatively decreased tracer uptake in AD patients compared to controls revealed several foci of statistical significance located in the white-matter compartment (Figure 4). Voxels of peak statistical difference between groups (significant at the $p_{FWE} < 0.05$ level, corrected for multiple comparisons), displayed in Table 3, were located bilaterally in the posterior hippocampal region, bilaterally in the splenium and in the genu of the corpus callosum, cingulum, right posterior limb of the internal capsule, and bilaterally in the pons.

Individual classification of subjects according to PIB positivity criteria

In the AD group, 14 patients (83%) were rated as positive for the presence of cortical amyloid deposition based on visual analyses assisted by automated methods. In the control group, six individuals (31%) were rated as PIB-positive.

Discussion

When intensity normalization was performed using cerebellar tracer uptake, the voxel-based analysis performed in this study showed broadly increased cortical ^{11}C-PIB uptake in the AD group as compared to healthy elderly controls, affecting orbitofrontal, parietal, and temporal areas most prominently. When intensity normalization was performed using proportional scaling to highlight the brain areas of greatest cortical binding of the tracer, the highest relative ^{11}C-PIB uptake was detected in the orbitofrontal cortex. Also when data were normalized to global brain uptake, the voxel-based approach allowed us to identify areas of significantly lower tracer uptake in specific white-matter tracts in AD patients relative to controls, a finding not reported in previous ^{11}C-PIB PET studies.

The findings of increased ^{11}C-PIB uptake across several portions of the cerebral cortex in patients with AD are consistent with the results of previous voxel-based analyses of ^{11}C-PIB PET data regarding both the topography of findings and the intensity of amyloid deposition, with small variations. This was shown in several previous reports using SPM and normalization to cerebellar uptake,[5] as well as in a few studies using proportional

Figure 1 Findings of increased carbon-11 labeled Pittsburgh compound B (^{11}C-PIB) uptake in patients with Alzheimer's disease (n=17) in comparison with healthy elderly controls (n=19) after cerebellum gray-matter normalization, highlighted in yellow (at the z >3.09 cutoff, corresponding to $p < 0.001$ uncorrected for multiple comparisons, and using an extent threshold of 10 voxels). Findings are overlaid on axial brain slices spatially normalized into an approximation to the Talairach and Tournoux stereotactic atlas,[30] and the numbers associated with each frame represent standard coordinates in the z-axis. Clusters of increased ^{11}C-PIB uptake are shown throughout the cerebral cortex. R = right side.

to tracer uptake in the cerebellum (Table 2). The highest statistical significance was attained for a large cluster (> 300 voxels) located in the left orbitofrontal cortex; five additional, less extensive clusters (>50 voxels) retained statistical significance, located respectively in the right inferior, left superior, and left inferior temporal gyri; right superior parietal lobule; and right orbitofrontal cortex (Table 3).

Typical patterns of ^{11}C-PIB uptake in AD and control subjects are shown in Figure 3, with two illustrative PET images showing different normalization methods and their respective time-activity curves (TACs). TACs illustrate the

Table 2 Comparisons of carbon-11 labeled Pittsburgh compound B (^{11}C-PIB) uptake between patients with Alzheimer's disease (n=17) and healthy controls (n=19), with normalization to cerebellar tracer uptake

Brain regions (Brodmann area)	Voxels* (n)	Coordinates[†] (x, y, z)	Peak z score[‡]	p-value[§]
Greater uptake in patients with Alzheimer's disease				
Right superior parietal lobule (7)	55	18, -50, 70	5.08	0.003
Left orbitofrontal cortex (10/11/47)	339	-18, 44, -20	4.93	0.006
Left superior temporal gyrus (38)	255	-50, 12, -26	4.93	0.006
Right inferior temporal gyrus (6/37)	292	40, -4, -44	4.89	0.008
Right middle temporal gyrus (21)	34	64, -12, -22	4.84	0.009
Left supplementary motor area (6)	23	-4, -12, 56	4.82	0.010
Left angular gyrus (39)	20	-48, -60, 44	4.70	0.017
Right postcentral gyrus (1)	59	64, -10, 22	4.70	0.017
Right fusiform gyrus (37)	59	40, -32, -24	4.69	0.018
Left inferior temporal gyrus (20)	45	-48, -14, -38	4.68	0.018
Right superior temporal gyrus (22)	88	68, -20, 2	4.67	0.019
Left middle temporal gyrus (21)	32	-62, -22, -18	4.64	0.021
Right orbitofrontal cortex (10)	66	40, 48, -14	4.57	0.028
Greater uptake in controls				
None				

* Number of contiguous voxels included in each cluster of between-group difference.
[†] Montreal Neurological Institute (MNI) coordinates of the voxel of maximal statistical significance within each cluster.
[‡] z scores for the voxel of maximal statistical significance in each cluster of between-group difference.
[§] Statistical significance after familywise error correction for multiple comparisons over the whole brain ($p < 0.05$, voxel level) and a minimum extent of 10 voxels.
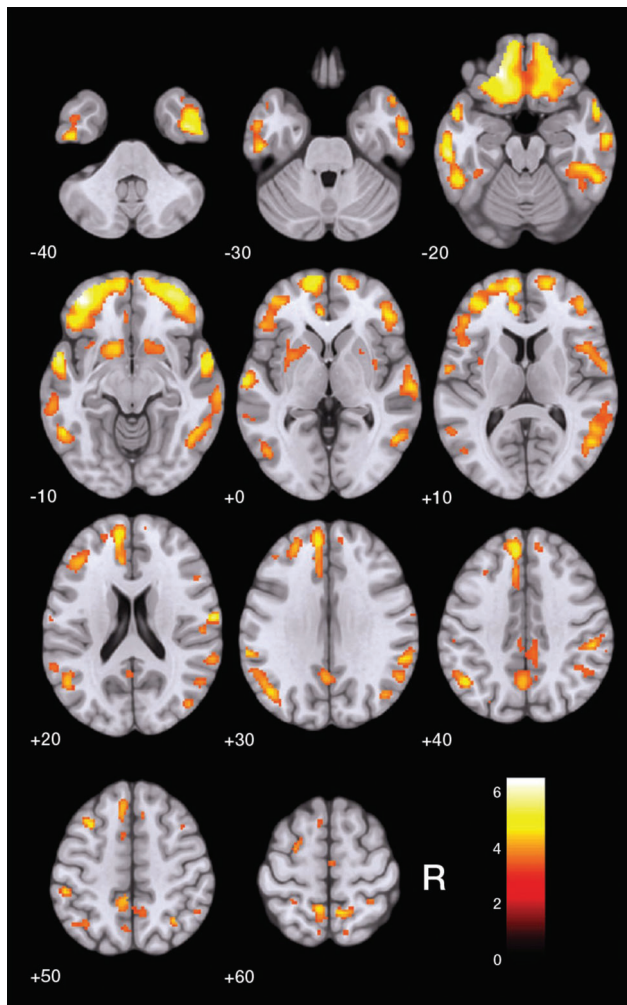
scaling/global mean normalization.[11] The present results, obtained in an AD sample with CDR values of 0.5 to 1, highlights the fact that prominent and diffuse amyloid deposition occurs very early over the course of AD. A pattern of high ^{11}C-PIB uptake in frontal areas, as well as in the temporal and parietal cortices, has been repeatedly reported since the first *in vivo* PET studies in humans[3] and has been validated for clinical use in several other ^{11}C-PIB PET studies using ROI-based analysis methods.[31]

The regional distribution of increased ^{11}C-PIB uptake within the frontal lobe in AD samples has been little addressed in previous PET investigations. Our findings indicate that, in the initial stages of AD, involvement of the frontal cortex is selective in orbital portions of this lobe. Buckner et al.[32] explored the relationship among amyloid deposition, atrophy, metabolism, and resting-state brain network activity. These authors suggested a possible link between neuronal activity in the default mode network (DMN) and the topography of amyloid deposition in AD.[31] Parts of the frontal cortex are highly active in the DMN, and this could explain higher amyloid deposition in frontal areas. However, Buckner et al.[32] focused on the overall pattern of amyloid distribution rather than on specific brain regions with peak tracer uptake. The reason why specific areas (i.e., the orbitofrontal cortex seen in the present work) would have higher deposition of amyloid is still unexplained. Sepulcre et al.[33] proposed a network-based spreading from limbic regions to the orbitofrontal cortex as being responsible for the initial topography of amyloid deposition load, which would then spread to other highly active areas of the brain, such as the DMN regions. Fjell et al.[34] recently reviewed the role of amyloid deposition in brain aging and AD, arguing in favor of the view that amyloid deposition may be more prominent in brain regions of higher local neuronal activity. However, it is relevant to note that there are no significant associations between deposition of amyloid in frontal areas and AD-related signs of neurodegeneration, such as cortical atrophy in the frontal cortex.[34] More prominent associations with signs of neurodegeneration are seen in lateral temporal and medial parietal areas.[34] Therefore, the prominence of amyloid deposition in the orbitofrontal cortex, as detected in the present study, highlights the view that extracellular amyloid plaques, particularly in frontal areas, may not be the sole (or more critical) trigger for typical AD-related neurodegenerative processes.[34] Such AD-related neurodegenerative changes in brain regions other than the frontal cortex may be more directly linked to other intracellular pathological processes, such as the accumulation of prefibrillar soluble amyloid oligomers or tau neurofibrillary tangles.[35]

We aimed to explore the potential benefit of the global mean normalization approach in ^{11}C-PIB-PET analyses to detect voxels with changes above the average uptake, depicting areas with the highest intensity of tracer uptake and, consequently, a more specific pattern in a given disease. It is known, for example, that variant forms of AD such as posterior cortical atrophy may feature a variable higher amyloid deposition in the occipital cortex.[36] Also, Parkinson's disease or dementia with Lewy bodies may feature spatial patterns of amyloid distribution distinct from those of the sporadic form of AD.[37] A method for intensity normalization with higher specificity, such as the global normalization approach, may be of special interest in those cases and may help differentiate these dementing conditions based on the topography of amyloid deposition. The findings presented herein suggest that the orbitofrontal cortex may be a key brain region for such differentiation. This possibility, however, needs to be confirmed in subsequent ^{11}C-PIB PET investigations.

The use of whole brain-based methods for local intensity normalization of brain PET data has raised methodological doubts in previous studies.[38] For instance, when

As in many previous imaging investigations of dementia, we categorized subjects as patients with AD or healthy controls on the basis of clinical data. Recently, the NIA-AA has launched a framework which aims to redefine AD for research purposes as a biological construct, using currently available biomarker data for Aβ deposition, pathologic tau, and neurodegeneration.[19] However, based on visual analyses of our individual datasets by two experienced nuclear medicine physicians assisted by automated methods,[29] we found that three out of 17 AD patients (17%) were rated as negative for the presence of cortical amyloid deposition (PIB-negative). Based on the current NIA-AA research framework, the term AD would not be applicable to such individuals.[19] Also, six out of 19 controls (31%) in our investigation were rated as presenting cortical amyloid deposition (PIB-positive). Therefore, as usually reported in the ^{11}C-PIB PET literature, not all AD patients are definitely PIB-positive and not all control individuals are definitely PIB-negative.[28,40] There are also various attempts to standardize the threshold for clinical "positivity" of PIB-PET,[41] and this issue is still an ongoing discussion. This is consistent with the current notion that Aβ pathology and cognitive abnormalities are not necessarily linearly associated with each other in the different phases of the disease. This association also changes according to the presence or absence of signs of neuronal damage.[40,42]

Our results also showed several foci of lower tracer uptake in white matter in patients with AD relative to controls, encompassing the corpus callosum, parahippocampus, cingulum, internal capsule, and pons. Although uptake of ^{11}C-PIB is known to occur in white-matter regions, its exact binding sites have not been defined yet. Initial publications suggested that white-matter uptake of ^{11}C-PIB should be seen as nonspecific binding.[3,4] However, since 2011, some studies have shown that ^{11}C-PIB uptake in the white matter could be related to myelin binding,[13] potentially opening a whole new field of application for this tracer. The decreased level of uptake of ^{11}C-PIB in the white matter detected in the AD group in our study is unlikely to be related to tracer distribution (i.e., kinetics of the tracer in the brain) due to its higher affinity for gray matter. This view is supported by the fact that uptake, retention, and clearance of ^{11}C-PIB in white matter are similar in AD patients and healthy controls.[3] While the pattern of decreased white matter ^{11}C-PIB PET uptake emerged most consistently with data normalized to global brain uptake, the same white-matter clusters also emerged in the between-group comparison with data normalized to cerebellar uptake (although they did not survive correction for multiple comparisons).

However, the fact that foci of decreased white-matter ^{11}C-PIB PET uptake in AD patients were detected by both intensity normalization methods suggests that such white-matter findings are not an artifact induced by AD-related variations in the reference measures used for normalization. Moreover, the presence and topographical distribution of our findings of relatively reduced ^{11}C-PIB uptake in the white-matter compartment are consistent with results of studies using diffusion tensor imaging (DTI)

Figure 2 Findings of increased carbon-11 labeled Pittsburgh compound B (^{11}C-PIB) uptake in patients with Alzheimer's disease (n=17) in comparison with healthy elderly controls (n=19) after global brain normalization, highlighted in yellow (at the z > 3.09 cutoff, corresponding to p < 0.001 uncorrected for multiple comparisons, and using an extent threshold of 10 voxels). Findings are overlaid on axial brain slices spatially normalized into an approximation to the Talairach and Tournoux stereotactic atlas,[30] and the numbers associated with each frame represent standard coordinates in the z-axis. Clusters are shown in several portions of the cerebral cortex, with the greatest size and statistical significance in the orbitofrontal cortex (Table 3). R = right side.

a group of patients exhibits globally decreased brain activity (as in AD, Parkinson's disease, and other neurodegenerative disorders), between-group comparisons against healthy individuals using globally normalized FDG-PET or regional cerebral blood flow data may display brain regions that artifactually appear hyperfunctional in patients relative to controls.[38,39] Therefore, we cannot definitely exclude the possibility that our findings of lower PIB uptake in AD patients relative to controls, saliently uncovered when we used the whole-brain normalization approach, may have been at least partially artifactual.

Table 3 Comparisons of carbon-11 labeled Pittsburgh compound B (^{11}C-PIB) uptake between patients with Alzheimer's disease (n=17) and healthy controls (n=19), with normalization to global uptake in the brain

| Brain regions (Brodmann area)	Voxels* (n)	Coordinates[†] (x, y, z)	Peak z score[‡]	p-value[§]
Greater uptake in patients with Alzheimer's disease				
Left orbitofrontal cortex (10/11)	324	-20, 38, -18	5.24	0.003
Right inferior temporal gyrus (20)	21	42, -4, -42	5.12	0.006
Right superior parietal gyrus (07)	25	16, -50, 68	4.94	0.013
Left superior temporal gyrus (22)	17	-56, 4, -12	4.87	0.018
Right orbitofrontal cortex (10)	44	18, 58, -14	4.84	0.020
Left inferior temporal gyrus (21)	13	-60, -26, -20	4.84	0.020
Greater uptake in controls				
Left hippocampal white matter	111	-24, -34, -8	5.54	0.001
Right hippocampal white matter	25	26, -28, -12	5.15	0.005
Right posterior cingulum	45	4, -38, 24	5.05	0.008
Right posterior limbic of the internal capsule	62	18, -10, 16	4.99	0.011
Genu of the corpus callosum	98	14, 32, -2	4.96	0.012
Splenium of the corpus callosum	26	-10, -40, 14	4.77	0.026
Left retrolenticular part of the internal capsule	16	-24, -30, 8	4.73	0.031

* Number of contiguous voxels included in each cluster of between-group difference.
[†] Montreal Neurological Institute (MNI) coordinates of the voxel of maximal statistical significance within each cluster.
[‡] z scores for the voxel of maximal statistical significance in each cluster of between-group difference.
[§] Statistical significance after familywise error correction for multiple comparisons over the whole brain (p < 0.05, voxel level) and a minimum extent of 10 voxels.
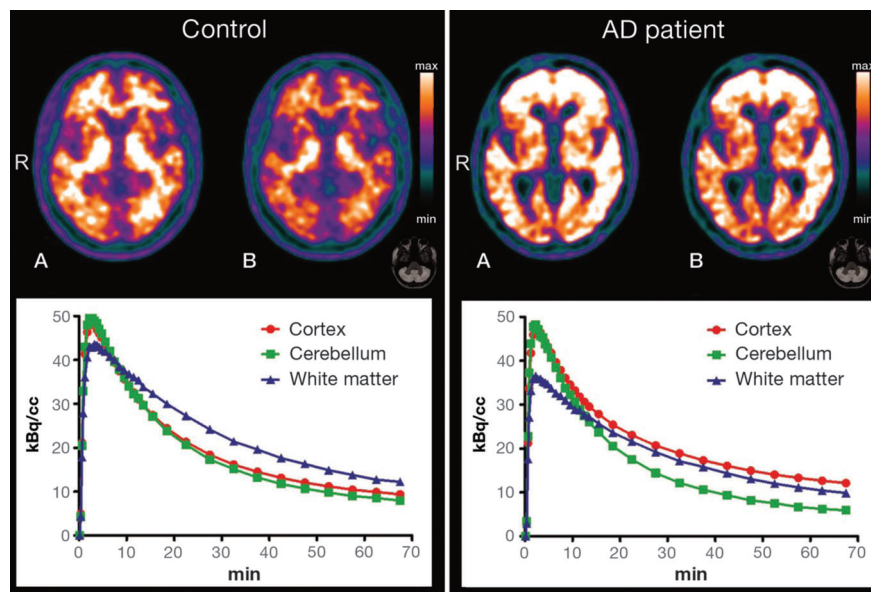

Figure 3 Illustrative positron emission tomography (PET) with carbon-11 labeled Pittsburgh compound B (^{11}C-PIB) images (top) are shown for a healthy control subject (left-side) and an AD patient (right-side) with regional tracer uptake data normalized either to total PIB uptake in the brain (A) or to cerebellar grey-matter uptake (B). The respective time-activity curves are shown at the bottom. AD = Alzheimer's disease; R = right side.

and morphometric MRI investigations comparing AD samples to healthy controls.[12] Corpus callosum atrophy has been detected in several MRI studies of AD, in direct proportion to the degree of cognitive decline.[43] Decreased fractional anisotropy in the parahippocampal white matter has been previously associated with cognitive impairment in DTI studies[44,45] and might reflect a demyelination process in AD.[44] This potential AD-related neuropathological process could be directly associated to our findings of decreased ^{11}C-PIB uptake in the parahippocampal white matter. Studies using DTI methods have also reported changes in the parahippocampal white matter of clinically

normal individuals with increased risk for AD[46] and in the cingulum in individuals with MCI.[45]

The two groups investigated herein had significant differences in educational attainment, with fewer years of formal education in the AD group. We refrained from repeating our between-group PET comparisons using an ANCOVA model with years of education as a covariate, given that we cannot affirm that the significant difference in years of formal education between AD patients and controls arose by chance.[47] However, despite this limitation, it is highly unlikely that the widespread between-group differences in PIB uptake reported herein would
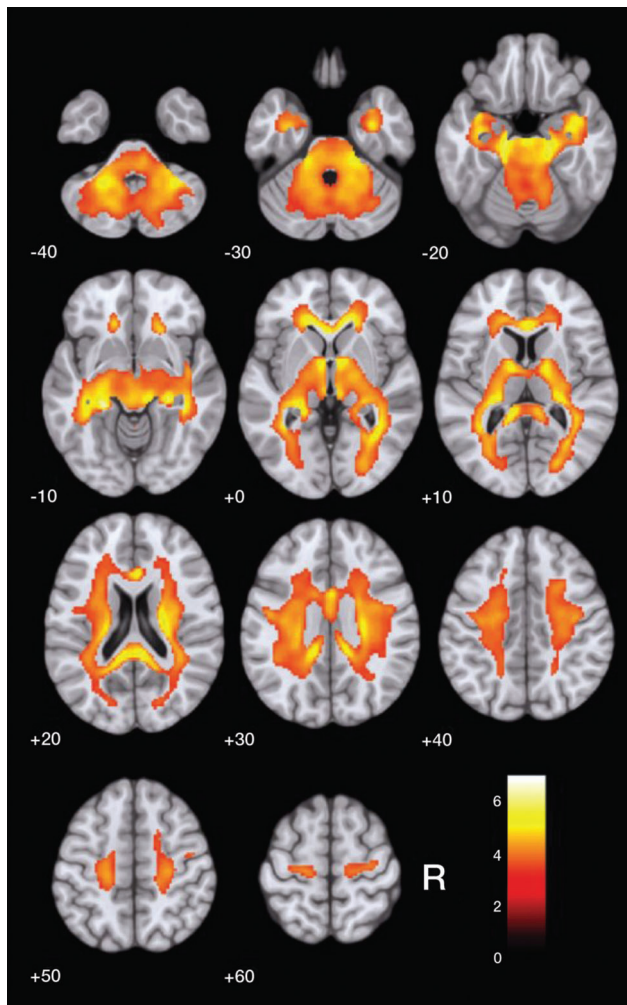
Figure 4 Findings of decreased carbon-11 labeled Pittsburgh compound B (^{11}C-PIB) uptake in patients with Alzheimer's disease (n=17) compared with healthy elderly controls (n=19) after global brain uptake normalization, highlighted in yellow (at the z > 3.09 cutoff, uncorrected for multiple comparisons and using an extent threshold of 10 voxels). Findings are overlaid on axial brain slices spatially normalized into an approximation to the Talairach and Tournoux stereotactic atlas,[30] and the numbers associated with each frame represent standard coordinates in the z-axis. Clusters are shown throughout the cerebral white matter. R = right side.

have emerged simply as a reflection of group differences in educational level. Alternatively, one might at most suggest that our findings might have been somehow amplified by the lower level of education of the AD group. This proposition would be consistent with the known moderating effect of education on the emergence and severity of clinical features of dementia in the presence of AD-related neurodegenerative changes,[48] as well as with the recently reported direct relationship between high education and low Aβ deposition as assessed with ^{11}C-PIB PET.[49]

There has been huge variation in the methods used for data acquisition and quantification in Aβ PET imaging studies to date. For instance, a number of PET studies

have used ^{11}C-PIB uptake data collected between 50 and 70 minutes after tracer injection,[41] while others have used data acquired between 40 and 60 minutes[29] or 40 to 70 minutes,[21,50] as in the present study. Also, some recent studies have normalized ^{11}C-PIB PET data to uptake specifically in the cerebellar crus[29] rather than the cerebellar gray matter, as in our study. Major international efforts are underway to standardize the results of quantitative measurements of Aβ tracers using PET, such as the Centiloid Project.[41] However, it is important to stress that the present study did not aim to contribute to such standardization efforts by carrying out comparisons of different methods; instead, we wished to take advantage of the characteristics of two different methods of intensity normalization to better document the topographical distribution of the cortical sites with highest tracer uptake in AD subjects with very mild or mild dementia.

One methodological strength of the present study regards the use of methods for partial volume correction of ^{11}C-PIB PET data, an approach recently demonstrated to improve accuracy for detection of abnormal cortical amyloid deposition.[23] On the other hand, one methodological limitation that must be acknowledged is our small sample size, which increases the risk of type II statistical errors. Nevertheless, highly significant foci of between-group differences in cortical ^{11}C-PIB uptake were detected, thus highlighting the sensitivity of ^{11}C-PIB-PET imaging to uncover widespread patterns of amyloid deposition in subjects with AD.

In conclusion, the present case-control voxelwise comparison of ^{11}C-PIB uptake in the brain highlighted the regional distribution of amyloid deposition in the cerebral cortex of AD patients, emphasizing the highest uptake detected in orbital portions of the frontal cortex. In addition, we report preliminary evidence of decreased ^{11}C-PIB uptake in white-matter regions in AD patients, suggesting that PET imaging with ^{11}C-PIB might be useful to identify white-matter damage in AD. The latter possibility should be further explored in future multimodal imaging studies examining the same AD patients and healthy controls, using both ^{11}C-PIB PET and DTI protocols with MRI.

Acknowledgements

Disclosure

The authors report no conflicts of interest.

References

1 Toussaint PJ, Perlbarg V, Bellec P, Desarnaud S, Lacomblez L, Doyon J, et al. Resting state FDG-PET functional connectivity as an early biomarker of Alzheimer's disease using conjoint univariate and independent component analyses. Neuroimage. 2012;63:936-46.

2 Mosconi L, Tsui WH, Herholz K, Puri A, Drzezga A, Lucignani G, et al. Multicenter standardized 18F-FDG PET diagnosis of mild cognitive impairment, Alzheimer's disease, and other dementias. J Nucl Med. 2008;49:390-8.

3 Klunk WE, Engler H, Nordberg A, Wang Y, Blomqvist G, Holt DP, et al. Imaging brain amyloid in Alzheimer's disease with Pittsburgh compound-B. Ann Neurol. 2004;55:306-19.

4 Price JC, Klunk WE, Lopresti BJ, Lu X, Hoge JA, Ziolko SK, et al. Kinetic modeling of amyloid binding in humans using PET imaging and Pittsburgh compound-B. J Cereb Blood Flow Metab. 2005;25: 1528-47.

5 Drzezga A, Grimmer T, Henriksen G, Stangier I, Perneczky R, Diehl-Schmid J, et al. Imaging of amyloid plaques and cerebral glucose metabolism in semantic dementia and Alzheimer's disease. Neuroimage. 2008;39:619-33.

6 Dukart J, Mueller K, Horstmann A, Vogt B, Frisch S, Barthel H, et al. Differential effects of global and cerebellar normalization on detection and differentiation of dementia in FDG-PET studies. Neuroimage. 2010;49:1490-5.

7 Küntzelmann A, Guenther T, Haberkorn U, Essig M, Giesel F, Henze R, et al. Impaired cerebral glucose metabolism in prodromal Alzheimer's disease differs by regional intensity normalization. Neurosci Lett. 2013;534:12-7.

8 Aalto S, Scheinin NM, Kemppainen NM, Någren K, Kailajärvi M, Leinonen M, et al. Reproducibility of automated simplified voxel-based analysis of PET amyloid ligand [11C]PIB uptake using 30-min scanning data. Eur J Nucl Med Mol Imaging. 2009;36:1651-60.

9 Lopresti BJ, Klunk WE, Mathis CA, Hoge JA, Ziolko SK, Lu X, et al. Simplified quantification of Pittsburgh compound B amyloid imaging PET studies: a comparative analysis. J Nucl Med. 2005;46: 1959-72.

10 Yamane T, Ishii K, Sakata M, Ikari Y, Nishio T, Ishii K, et al. Inter-rater variability of visual interpretation and comparison with quantitative evaluation of ^{11}C-PiB PET amyloid images of the Japanese Alzheimer's disease neuroimaging initiative (J-ADNI) multicenter study. Eur J Nucl Med Mol Imaging. 2017;44:850-7.

11 Shin J, Lee SY, Kim SJ, Kim SH, Cho SJ, Kim YB. Voxel-based analysis of Alzheimer's disease PET imaging using a triplet of radiotracers: PIB, FDDNP, and FDG. Neuroimage. 2010;52: 488-96.

12 Radanovic M, Pereira FR, Stella F, Aprahamian I, Ferreira LK, Forlenza OV, et al. White matter abnormalities associated with Alzheimer's disease and mild cognitive impairment: a critical review of MRI studies. Expert Rev Neurother. 2013;13:483-93.

13 Stankoff B, Freeman L, Aigrot MS, Chardain A, Dollé F, Williams A, et al. Imaging central nervous system myelin by positron emission tomography in multiple sclerosis using [methyl-11C]-2-(4'-methylaminophenyl)- 6-hydroxybenzothiazole. Ann Neurol. 2011;69:673-80.

14 Maia ALG, Godinho C, Ferreira ED, Almeida V, Schuh A, Kaye J, et al. Aplicação da versão brasileira da escala de avaliação clínica da demência (Clinical Dementia Rating – CDR) em amostras de pacientes com demência. Arq Neuropsiquiatr. 2006;64:485-9.

15 McKhann GM, Knopman DS, Chertkow H, Hyman BT, Jack CR Jr, Kawas CH, et al. The diagnosis of dementia due to Alzheimer's disease: recommendations from the national institute on aging-Alzheimer's association workgroups on diagnostic guidelines for Alzheimer's disease. Alzheimers Dement. 2011;7:263-9.

16 Del-Ben CM, Vilela JAA, Crippa JAS, Hallak JEC, Labate CM, Zuardi AW. Confiabilidade da "Entrevista Clínica Estruturada para o DSM-IV – Versão Clínica" traduzida para o português. Rev Bras Psiquiatr. 2001;23:159-9.

17 Blessed G, Tomlinson BE, Roth M. The association between quantitative measures of dementia and senile change in the cerebral grey matter of elderly subjects. Br J Psychiatry. 1968;114:797-811.

18 Brucki SM, Nitrini R, Caramelli P, Bertolucci PH, Okamoto IH. [Suggestions for utilization of the mini-mental state examination in Brazil]. Arq Neuropsiquiatr. 2003;61:777-81.

19 Jack CR Jr, Bennett DA, Blennow K, Carrillo MC, Dunn B, Haeberlein SB, et al. NIA-AA research framework: toward a biological definition of Alzheimer's disease. Alzheimers Dement. 2018;14:535-62.

20 Harris PA, Taylor R, Thielke R, Payne J, Gonzalez N, Conde JG. Research electronic data capture (REDCap) – a metadata-driven methodology and workflow process for providing translational research informatics support. J Biomed Inform. 2009;42:377-81.

21 Benzinger TL, Blazey T, Jack CR Jr, Koeppe RA, Su Y, Xiong C, et al. Regional variability of imaging biomarkers in autosomal dominant Alzheimer's disease. Proc Natl Acad Sci U S A. 2013;110: E4502-9.

22 Thomas BA, Erlandsson K, Modat M, Thurfjell L, Vandenberghe R, Ourselin S, et al. The importance of appropriate partial volume correction for PET quantification in Alzheimer's disease. Eur J Nucl Med Mol Imaging. 2011;38:1104-19.

23 Matsubara K, Ibaraki M, Shimada H, Ikoma Y, Suhara T, Kinoshita T, et al. Impact of spillover from white matter by partial volume effect on quantification of amyloid deposition with [11C]PiB PET. Neuroimage. 2016;143:316-24.

24 Meltzer CC, Cantwell MN, Greer PJ, Ben-Eliezer D, Smith G, Frank G, et al. Does cerebral blood flow decline in healthy aging? A PET study with partial-volume correction. J Nucl Med. 2000;41:1842-8.

25 Quarantelli M, Berkouk K, Prinster A, Landau B, Svarer C, Balkay L, et al. Integrated software for the analysis of brain PET/SPECT studies with partial-volume-effect correction. J Nucl Med. 2004;45:192-201.

26 Ashburner J. A fast diffeomorphic image registration algorithm. Neuroimage. 2007;38:95-113.

27 Ashburner J, Friston KJ. Unified segmentation. Neuroimage. 2005; 26:839-51.

28 Hosokawa C, Ishii K, Hyodo T, Sakaguchi K, Usami K, Shimamoto K, et al. Investigation of 11C-PiB equivocal PET findings. Ann Nucl Med. 2015;29:164-9.

29 Jack CR Jr, Wiste HJ, Weigand SD, Therneau TM, Lowe VJ, Knopman DS, et al. Defining imaging biomarker cut points for brain aging and Alzheimer's disease. Alzheimers Dement. 2017;13:205-16.

30 Talairach J, Tornoux P. A Co-planar stereotaxic atlas of human brain. Stuttgart: Thieme1988.

31 Edison P, Carter SF, Rinne JO, Gelosa G, Herholz K, Nordberg A, et al. Comparison of MRI based and PET template based approaches in the quantitative analysis of amyloid imaging with PIB-PET. Neuroimage. 2013;70:423-33.

32 Buckner RL. The serendipitous discovery of the brain's default network. Neuroimage. 2012;62:1137-45.

33 Sepulcre J, Sabuncu MR, Becker A, Sperling R, Johnson KA. In vivo characterization of the early states of the amyloid-beta network. Brain. 2013;136:2239-52.

34 Fjell AM, McEvoy L, Holland D, Dale AM, Walhovd KB; Alzheimer's Disease Neuroimaging Initiative. What is normal in normal aging? Effects of aging, amyloid and Alzheimer's disease on the cerebral cortex and the hippocampus. Prog Neurobiol. 2014;117:20-40.

35 Sakono M, Zako T. Amyloid oligomers: formation and toxicity of Abeta oligomers. FEBS J. 2010;277:1348-58.

36 Formaggio M, Costes N, Seguin J, Tholance Y, Le Bars D, Roullet-Solignac I, et al. In vivo demonstration of amyloid burden in posterior cortical atrophy: a case series with PET and CSF findings. J Neurol. 2011;258:1841-51.

37 Gomperts SN, Rentz DM, Moran E, Becker JA, Locascio JJ, Klunk WE, et al. Imaging amyloid deposition in Lewy body diseases. Neurology. 2008;71:903-10.

38 Borghammer P, Aanerud J, Gjedde A. Data-driven intensity normalization of PET group comparison studies is superior to global mean normalization. Neuroimage. 2009;46:981-8.

39 Duran FL, Zampieri FG, Bottino CC, Buchpiguel CA, Busatto GF. Voxel-based investigations of regional cerebral blood flow abnormalities in Alzheimer's disease using a single-detector SPECT system. Clinics (Sao Paulo). 2007;62:377-84.

40 Pike KE, Savage G, Villemagne VL, Ng S, Moss SA, Maruff P, et al. Beta-amyloid imaging and memory in non-demented individuals: evidence for preclinical Alzheimer's disease. Brain. 2007;130:2837-44.

41 Klunk WE, Koeppec RA, Priced JC, Benzingere TL, Devous MD Sr, Jagust WJ, et al. The Centiloid project: standardizing quantitative amyloid plaque estimation by PET. Alzheimers Dement. 2015;11: 1-15.e1-4.

42 Mormino EC, Betensky RA, Hedden T, Schultz AP, Amariglio RE, Rentz DM, et al. Synergistic effect of β-amyloid and neurodegeneration on cognitive decline in clinically normal individuals. JAMA Neurol. 2014;71:1379-85.

43 Griebe M, Förster A, Wessa M, Rossmanith C, Bäzner H, Sauer T, et al. Loss of callosal fiber integrity in healthy elderly with age-related white matter changes. J Neurol. 2011;258:1451-9.

44 Wang PN, Chou KH, Liang JF, Lin KN, Chen WT, Lin CP. Multiple diffusivities define white matter degeneration in amnestic mild cognitive impairment and Alzheimer's disease. J Alzheimers Dis. 2012;30:423-37.

45 Zhang Y, Schuff N, Jahng GH, Bayne W, Mori S, Schad L, et al. Diffusion tensor imaging of cingulum fibers in mild cognitive impairment and Alzheimer disease. Neurology. 2007;68:13-9.

46 Rieckmann A, Van Dijk KR, Sperling RA, Johnson KA, Bucker RL, Hedden T. Accelerated decline in white matter integrity in clinically normal individuals at risk for Alzheimer's disease. Neurobiol Aging. 2016;42:177-88.

47 Miller GA, Chapman JP. Misunderstanding analysis of covariance. J Abnorm Psychol. 2001;110:40-8.

48 Tom SE, Hubbard RA, Crane PK, Haneuse SJ, Bowen J, McCormick WC, et al. Characterization of dementia and Alzheimer's disease in an older population: updated incidence and life expectancy with and without dementia. Am J Public Health. 2015;105:408-13.

49 Yasuno F, Kazui H, Morita N, Kajimoto K, Ihara M, Taguchi A, et al. Low amyloid-β deposition correlates with high education in cognitively normal older adults: a pilot study. Int J Geriatr Psychiatry. 2015;30: 919-26.

50 Grimmer T, Riemenschneider M, Förstl H, Henriksen G, Klunk WE, Mathis CA, et al. Beta amyloid in Alzheimer's disease: increased deposition in brain is reflected in reduced concentration in cerebrospinal fluid. Biol Psychiatry. 2009;65:927-34.